CHEMICAL PHYSICS

Femtosecond symmetry breaking and coherent relaxation of methane cations via x-ray spectroscopy

Enrico Ridente[1,2]†, Diptarka Hait[1,2]†‡, Eric A. Haugen[1,2], Andrew D. Ross[1,2]§, Daniel M. Neumark[1,2], Martin Head-Gordon[1,2], Stephen R. Leone[1,2,3]*

Understanding the relaxation pathways of photoexcited molecules is essential to gain atomistic-level insight into photochemistry. We performed a time-resolved study of ultrafast molecular symmetry breaking through geometric relaxation (Jahn-Teller distortion) on the methane cation. Attosecond transient absorption spectroscopy with soft x-rays at the carbon K-edge revealed that the distortion occurred within 10 ± 2 femtoseconds after few-femtosecond strong-field ionization of methane. The distortion activated coherent oscillations in the asymmetric scissoring vibrational mode of the symmetry-broken cation, which were detected in the x-ray signal. These oscillations were damped within 58 ± 13 femtoseconds because vibrational coherence was lost with the energy redistributing into lower-frequency vibrational modes. This study completely reconstructs the molecular relaxation dynamics of this prototypical example and opens avenues for exploring complex systems.

Chemical reactions arise from the motion of atomic nuclei. Atomic displacements can be described in terms of either fluctuations about a local minimum of energy or relaxation toward such a minimum from a nonequilibrium configuration. The latter often results from interaction with light because photon absorption can lead to excited electronic states with minimum energy geometries quite distinct from the initial starting point. The nonequilibrium configurations arising from light-matter interaction thus can have substantial surplus potential energy, which can drive chemical transformations. Therefore, intramolecular relaxation dynamics of photoexcited molecules are of fundamental photochemical interest.

Jahn-Teller (JT) distortion (*1*, *2*) is a special type of relaxation mechanism that spontaneously reduces the spatial symmetry of nonlinear molecules in degenerate electronic states. Molecular geometries where multiple electronic states are isoenergetic are not stable for any of the associated states (*1*) and represent a fundamental breakdown of the Born-Oppenheimer approximation (*3*). It therefore becomes energetically favorable to undergo distortions that lift the degeneracy by breaking spatial symmetry. JT distortions are ubiquitous in solids (*4*) and gas-phase molecules (*5*). In this work, we used attosecond x-ray transient absorption spectroscopy (XTAS) to study symmetry breaking of the methane cation (CH_4^+) generated through vertical strong-field ionization (SFI). This work unequivocally revealed the role and timescale of JT-induced dynamics experimentally and provided an understanding of relaxation mechanisms in molecular systems.

CH_4^+ is a classic system in which JT distortions occur (*6*–*9*). The process starts with CH_4, which is the smallest stable molecule with tetrahedral (T_d) geometry. The equilibrium C-H bond distances are 1.087 Å (*10*), and all of the H-C-H bond angles are ≈109.5° because of T_d symmetry. The ground-state molecular orbitals (MOs) are shown in Fig. 1A, and the electronic configuration of neutral CH_4 is $1a_1^2 2a_1^2 1t_2^6$ ($^1A_1$). The electronic ground-state configuration of CH_4^+ at the T_d geometry is $1a_1^2 2a_1^2 1t_2^5$, which is triply degenerate ($^2T_2$) because each of the three $1t_2$ orbitals is equally likely to be singly occupied. Therefore, CH_4^+ undergoes JT distortion away from the T_d geometry to a lower symmetry C_{2v} form (*7*, *11*–*14*). This JT distortion involves t_2 and e symmetry vibrational modes of CH_4, making CH_4^+ the simplest $T_2 \otimes (t_2 + e)$ JT problem (*15*). The resulting C_{2v} equilibrium structure was computed to have two long (1.187 Å) and two short (1.083 Å) C-H bonds (Fig. 1A), which indicates antisymmetric stretching (t_2 symmetry) relative to neutral CH_4. The angle formed by the long C-H bonds is 55.0°, and the short bonds form an angle of 125.7°, representing considerable deviations from the initial T_d geometry through bending motions (of t_2 and e symmetry in CH_4). These distortions lower the energy of the doubly occupied $3a_1$ and $1b_1$ MOs (Fig. 1A) but also destabilize the $1b_2$ singly occupied MO (SOMO). The electronic ground state of CH_4^+ therefore is $^2B_2$ (*12*).

Molecular JT-distorted forms, and CH_4^+ in particular, have been extensively studied both theoretically (*15*–*18*) and experimentally (*6*, *19*). Experimentally, time resolving the JT distortion in CH_4^+ remained an open challenge (*7*, *13*) because of the ultrafast nature of the process. JT-distorted species have been characterized in photoelectron spectroscopy experiments (*6*, *20*), but such measurements lack the temporal resolution to obtain the femtosecond timescale dynamics of symmetry breaking. Baker *et al.* (*21*) used attosecond-resolution high-harmonic emission spectroscopy to report on the onset of the JT distortions in CH_4^+ and deuterated CD_4^+ up to the first 1.6 fs. The nuclear motion in those experiments, however, cannot be reconstructed at longer times, which precludes a complete analysis of the JT relaxation process and subsequent coherent motion. Coulomb explosion experiments by Li *et al.* (*22*) probed the dynamics of CH_4^+ by recording the photofragments after interaction with two time-delayed strong-field 800-nm pulses, but temporal resolution was limited by the 25-fs pulses used as pump and probe. Furthermore, their use of a multicycle pump pulse led to several additional photoproducts from higher-energy fragmentation pathways that compete with JT distortions. It has been shown that the use of shorter, few-cycle 800-nm pulses increased the relative amount of CH_4^+ by suppressing additional product channels (*23*).

XTAS, based on attosecond- and few-femtosecond-duration soft x-ray pulses generated through high-harmonic generation (*24*), has been successfully used to study ultrafast molecular relaxation processes with high structural and temporal resolution (*25*, *26*). XTAS at the carbon K-edge is therefore an ideal platform to observe few-femtosecond timescale dynamics such as those associated with the JT distortion of CH_4^+ (*27*, *28*). The x-ray probe excites C 1s electrons to unoccupied levels, such as the SOMO, or completely unoccupied antibonding or Rydberg levels. In particular, the dipole-allowed 1s → SOMO signal in CH_4^+ is expected to be energetically well resolved from other features. Geometric changes as a result of JT distortion will strongly affect the SOMO energy, which can be traced by XTAS with few-femtosecond time resolution.

In this work, we report a joint experimental and theoretical study of the symmetry-breaking JT dynamics of CH_4^+. The cations were produced from neutral methane through abrupt, few-femtosecond SFI of CH_4 with an 800-nm, few-cycle pump pulse generated by a table-top Ti:sapphire laser. The induced dynamics were then probed with XTAS using high-harmonic–generated soft x-ray pulses at the C K-edge obtained with a 1300-nm source (*24*). The nonperturbative nature of SFI leads to an ionization window that is temporally much narrower than the 5-fs width of the pump pulse (*29*). We observed a substantial energy shift in the XTAS signal immediately upon ionization because of JT distortion. The C_{2v} minimum geometry was

[1]Department of Chemistry, University of California, Berkeley, CA 94720, USA. [2]Chemical Sciences Division, Lawrence Berkeley National Laboratory, Berkeley, CA 94720, USA. [3]Department of Physics, University of California, Berkeley, CA 94720, USA.
*Corresponding author. Email: srl@berkeley.edu
†These authors contributed equally to this work.
‡Present address: Department of Chemistry and PULSE Institute, Stanford University, Stanford, CA 94305, USA.
§Present address: TOPTICA Photonics Inc., Pittsford, NY 14534, USA.

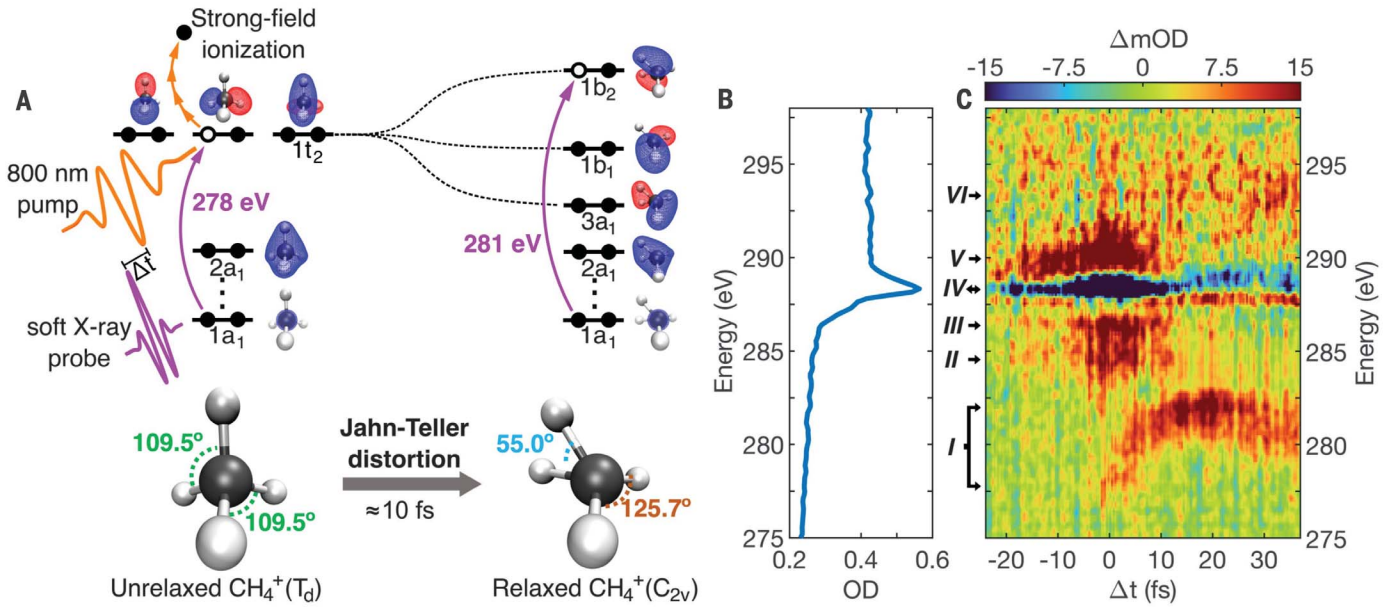

Fig. 1. XTAS measurements of CH_4^+ dynamics. (**A**) Schematic of the pump-probe process. Pump-induced SFI produces T_d symmetry CH_4^+, which undergoes JT distortion toward a C_{2v} minimum. MOs for both structures are also shown (energies not to scale). The $1a_1$ orbital is the C 1s core-level, and the remainder are $\sigma_{C\text{-}H}$ bonding orbitals. The dynamics are mapped by the 1s → SOMO probe transition induced by a time-delayed (Δt) soft x-ray probe. (**B**) Ground-state carbon K-edge x-ray absorption spectrum for CH_4. (**C**) Transient x-ray absorption at Δt < 35 fs. Negative time indicates probe preceding pump. The low-energy signal (278 to 282 eV) corresponds to the 1s → SOMO probe transition, which indicates that the C_{2v} minimum is reached by ≈10 fs.

attained within ≈10 fs, which was followed by two coherent oscillations in the signal that revealed large-amplitude scissoring motion. These coherent oscillations were damped out by ≈60 fs, indicating vibrational dephasing and eventual decoherence. The behavior of fully deuterated methane cations (CD_4^+) was also investigated to understand the effect of substituent masses on the JT dynamics.

General features of XTAS signal

CH_4 has a simple ground-state x-ray absorption spectrum (Fig. 1B). There is only one prominent peak (288 eV), which arises from the 1s → 3p Rydberg excitation (*30*). No other noteworthy pre-edge features were observed, and 1s ionization occurred at ≈290.8 eV (*31*).

Figure 1C shows the experimental carbon K-edge XTAS spectrum for CH_4^+ up to 35 fs after the pump pulse abruptly ionizes the molecule at time t = 0. The intensity of the pump beam was 3×10^{14} W/cm^2, which generated sufficient CH_4^+ without substantial photodissociation, as discussed in the supplementary materials. Previous investigations have confirmed that the major photoproduct for an 800-nm pump pulse of similar intensity and pulse duration is CH_4^+ (*32*). The negative (blue) transient signal (feature IV) corresponds to the depletion of neutral CH_4 and can be more clearly observed at higher values of the pump power (see the supplementary materials). At t = 0, other prominent features were the positive (red) signals at 278 to 282 eV (I), 284 eV (II), 287 eV (III), and 290 to 292 eV (V). The broad features II, III, and V had substantial temporal overlap with the pump pulse and could be attributed to the Stark effect of the pump pulse on core-excitation energies of CH_4 (supplementary materials). Their temporal width is longer than the pump pulse because the Stark shift in XTAS measurements is proportional to the cross-correlation and timing jitter between pump and probe. After t = 0, a positive feature at ≈287.5 eV could be observed. This feature arose because of Raman activation of the symmetric stretch vibrational mode of CH_4 by the pump pulse (supplementary materials), like the behavior that has been observed in other molecules (*33*, *34*).

Feature I was assigned to CH_4^+ on the basis of orbital-optimized density functional theory (OO-DFT) calculations (*35*) that revealed that this feature corresponded to the 1s → SOMO excitation of nonequilibrium T_d CH_4^+. OO-DFT indicated that other core-level excitations of CH_4^+ (such as 1s → σ* or the Rydberg levels) were above 288 eV in energy (supplementary materials). Feature VI in Fig. 1C corresponds to such excitations and could be observed at long times. However, feature VI did not show discernible time evolution. Conversely, feature I was well separated from all the other features and was particularly sensitive to changes in molecular geometry as the SOMO is of $\sigma_{C\text{-}H}$ character. The time evolution of this signal was the clearest reporter of the dynamics of CH_4^+, and the analysis below therefore focuses on it.

Relaxation dynamics of CH_4^+

The long-time experimental XTAS of the JT feature corresponding to the 1s → SOMO transition is given in Fig. 2A. The energetic average (henceforth abbreviated as CM1, for the first central moment) of the differential absorption [change in milli–optical density (ΔmOD)] signal (solid black line) showed three main characteristics. A rapid blue shift in energy from 278 eV (at t ≈ 0) to ≈282 eV (at t ≈ 18 fs) was followed by damped oscillations until t ≈ 60 fs and subsequently an almost time-independent signal between 281 and 281.5 eV. The width of the spectral feature increased considerably starting around t ≈ 10 fs, leading to a very broad signal at longer times.

We interpreted the behavior of this signal using quasiclassical ab initio molecular dynamics (AIMD) (*36*) trajectories on CH_4^+. Figure 2B shows the XTAS signal computed using OO-DFT from 255 AIMD trajectory geometries at different time points, revealing good agreement with the experimental results. This comparison indicates that the trajectories underlying the spectrum are a good reporter of the molecular dynamics under the experimental conditions. It is worth noting that all of the AIMD calculations were performed on the electronic ground state of CH_4^+ (i.e., were adiabatic). Nonadiabatic effects from higher-energy electronic states of CH_4^+ could potentially contribute to the small differences between experiment and theory, but the experimental evidence suggests that the system is always in

the ground electronic state under experimental conditions (supplementary materials). In general, no explicit signature of nonadiabaticity was observed in the experimental spectrum, as made evident by the good agreement between Fig. 2, A and B. The potential role of nonadiabatic effects on other aspects related to the JT distortion of CH_4 has been considered elsewhere (*9*, *15*–*18*).

The timescale for the JT process can be directly estimated by the time taken by the CM1 to attain the 281.5-eV value that we associate with the C_{2v} form of CH_4^+. This value was chosen because it corresponds to the asymptotic long-time limit of the experimental signal CM1, and this value was also estimated by OO-DFT to be the upper bound for the 1s → SOMO excitation of CH_4^+ at the C_{2v} equilibrium geometry (supplementary materials). This value was measured at 10 ± 2 fs from experiment by fitting an error function to the first 20 fs of the 1s → SOMO feature (supplementary materials). OO-DFT calculations find this time to be 9.4 ± 0.3 fs, confirming that JT relaxation occurs on a timescale associated with high-frequency vibrational motion.

In general, the time evolution of the signal corresponds to atomic motions associated with the relaxation process, with the oscillatory patterns suggesting involvement of vibrational modes of CH_4^+. This evolution could be analyzed further using a Fourier transform (FT) of the CM1 position from both theory and experiment (Fig. 2C). Even though the FT features were broad owing to the rapid decay in the oscillation amplitude, it was possible to identify critical frequencies. The most intense peak in the FT was at ≈1200 cm^{-1}, a frequency that corresponded to a computed normal mode of the C_{2v} minimum associated with scissoring about the H-C-H bond angles. This mode is an asymmetric scissoring mode (supplementary materials), where the scissoring motion about the smallest bond angle (i.e., the angle between the two long C-H bonds) is opposite in direction to the scissoring motion about the largest bond angle (i.e., the angle between the two short C-H bonds). However, caution must be taken in interpreting the FT features in terms of the fundamental frequencies of the C_{2v} minimum; the CH_4^+ ground-state surface has 12 distinct C_{2v} minima (*37*) and multiple seams corresponding to electronic state degeneracies, resulting in a highly anharmonic potential energy surface (PES). The FT is nonetheless an indication of several molecular motions that affect the signal and the associated timescales. The damping rate for the 1200 cm^{-1} frequency could also be estimated by fitting to the time domain experimental CM1 (Fig. 2D), revealing a lifetime of 58 ± 13 fs for the oscillations.

We used the AIMD trajectories to uncover the origins of the signal oscillations in the x-ray spectra. The trajectories indicated that the C-H

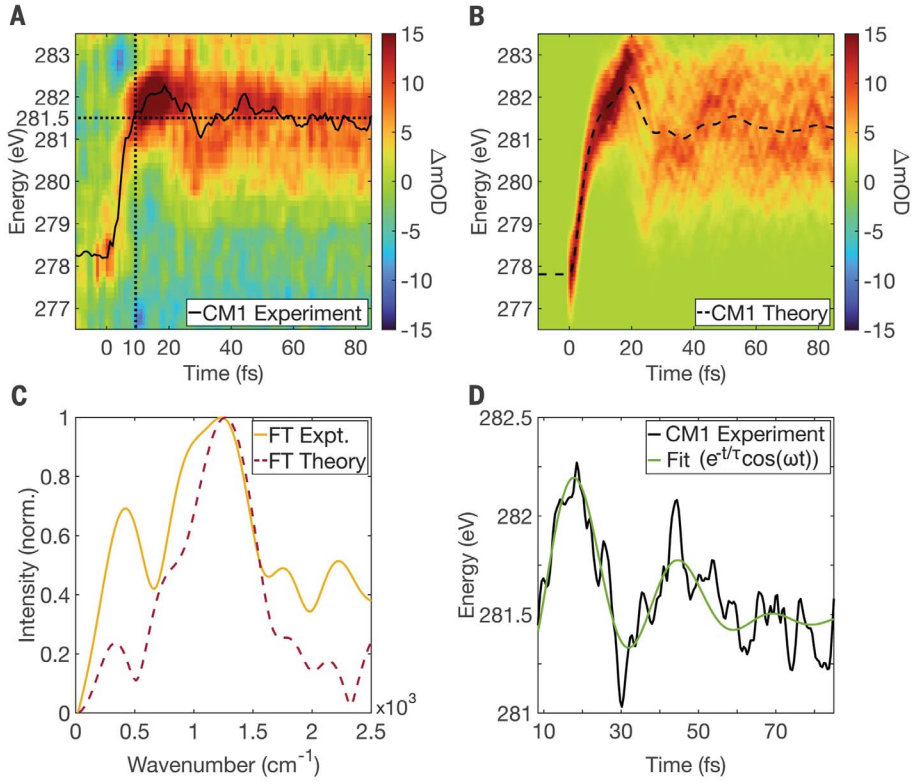

Fig. 2. Time evolution of the 1s → SOMO transition of CH_4^+. (**A**) Experimental XTAS for the 1s → SOMO transition of CH_4^+, with the first central moment (CM1) shown with the solid black line. The dotted black lines indicate the asymptotic long-time signal CM1 (281.5 eV), which corresponds to the vibrationally hot C_{2v} cation generated by the experiment, and at what time this energy is first reached (10 fs, JT timescale). (**B**) Theoretical XTAS for the same excitation. (**C**) FT of the CM1 from experiment (solid line) and theory (dashed line). The theoretical intensities have been uniformly scaled to match experiment for peak absorbance. (**D**) Experimental CM1 fit with $-e^{-t/\tau} \times \cos(\omega t)$, with ω = 1200 cm^{-1}, indicating a damping lifetime of τ = 58 ± 13 fs for the vibrational dephasing.

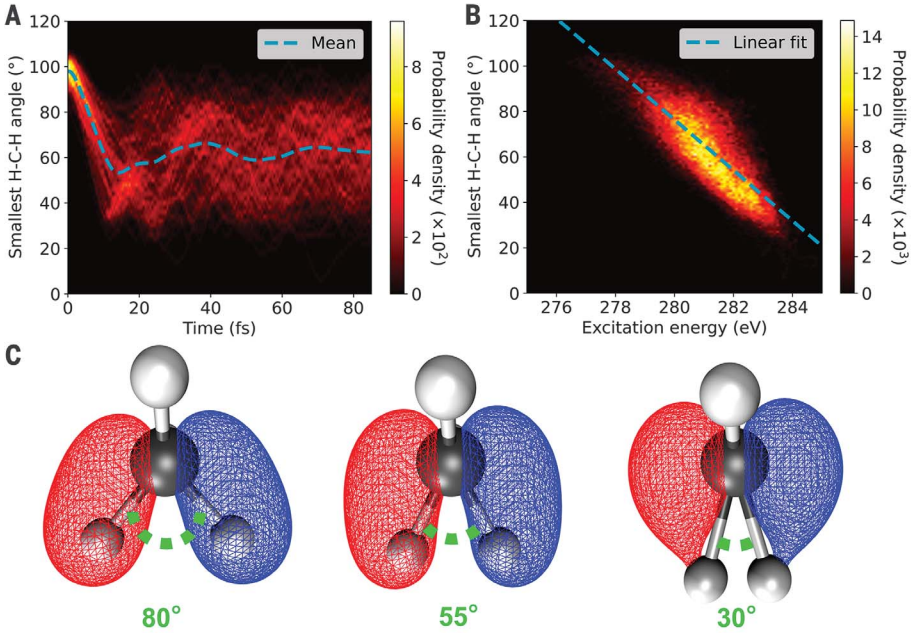

Fig. 3. Role of the smallest H-C-H angle on XTAS signal. (**A**) Time evolution of the smallest bond angle over the trajectories. (**B**) Correlation between the computed 1s → SOMO excitation energies versus the smallest bond angle of the corresponding structures. (**C**) Evolution of the SOMO with change in the smallest bond angle.

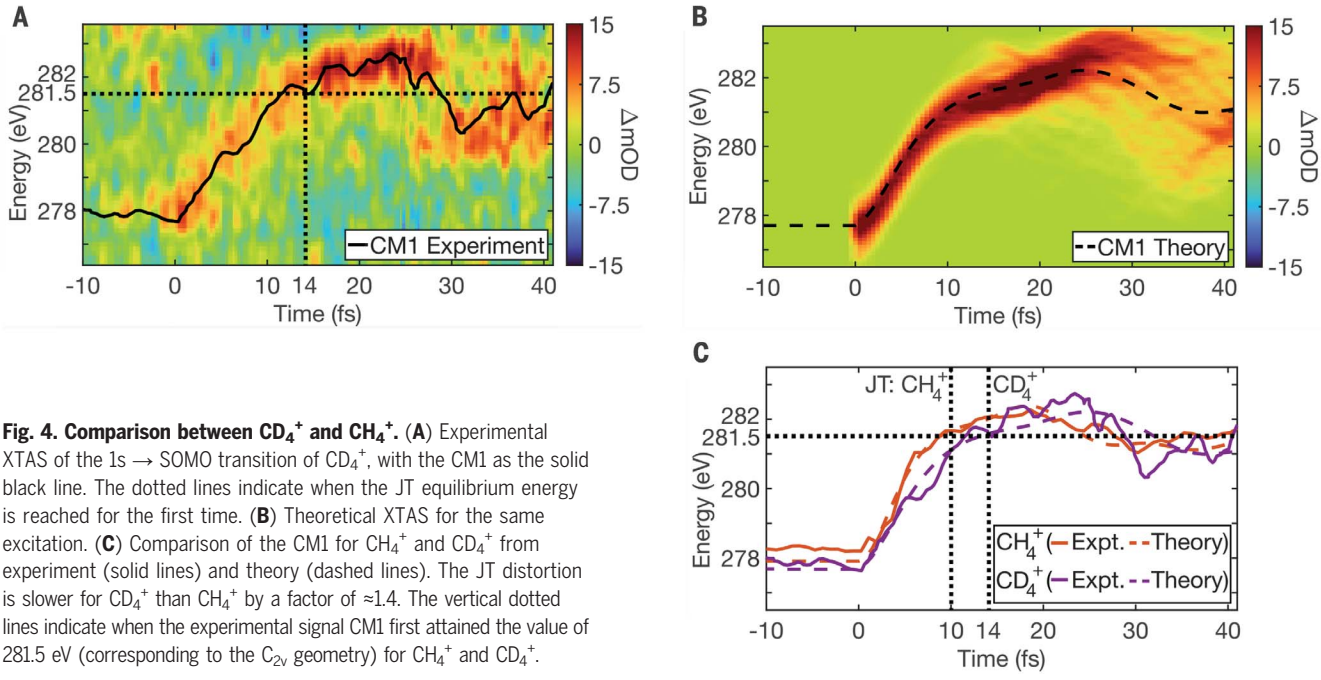

Fig. 4. Comparison between CD_4^+ and CH_4^+. (**A**) Experimental XTAS of the 1s → SOMO transition of CD_4^+, with the CM1 as the solid black line. The dotted lines indicate when the JT equilibrium energy is reached for the first time. (**B**) Theoretical XTAS for the same excitation. (**C**) Comparison of the CM1 for CH_4^+ and CD_4^+ from experiment (solid lines) and theory (dashed lines). The JT distortion is slower for CD_4^+ than CH_4^+ by a factor of ≈1.4. The vertical dotted lines indicate when the experimental signal CM1 first attained the value of 281.5 eV (corresponding to the C_{2v} geometry) for CH_4^+ and CD_4^+.

bond lengths oscillate on a timescale roughly twice as fast as the principal oscillation in the CM1 (supplementary materials). The angular oscillations were slower than the stretches, with Fig. 3A showing that the mean of the smallest molecular bond angle over all trajectories underwent a damped oscillatory motion on the same timescale as the predicted and observed XTAS signal CM1 (Fig. 2, A and B). The computed bond angle distribution also broadened rapidly over time after $t \approx 10$ fs, similar to the XTAS signal. A direct correlation between the observed signal and the smallest bond angle is revealed in Fig. 3B, which plots the smallest bond angle of the trajectory geometries used for Fig. 2B against the computed 1s → SOMO excitation energies for those geometries. It is evident that a simple linear model could capture much of the relationship between the two quantities. The excitation energy had weaker correlation with other bond angles and bond lengths (supplementary materials). Theory therefore indicated that the most important contribution to the observed time evolution of the XTAS absorption energy was from the dynamics of the smallest bond angle, to the extent that the signal could be interpreted in terms of a single parameter.

This connection can be understood using a simple orbital model (Fig. 3C). The SOMO at the C_{2v} symmetry minimum geometry of CH_4^+ is the bonding orbital arising from mixing between a C 2p orbital and a symmetry-adapted linear combination (SALC) of the 1s orbitals corresponding to H atoms in the long bonds. This SALC has antibonding character because the two H 1s orbitals have opposite phases. For small bond angles, the H 1s SALC has poorer overlap with the C 2p level as it gets closer to the nodal plane of the latter. This behavior leads to a weaker interaction and therefore lowers the mixing between the C and H centered orbitals. Furthermore, smaller angles lead to decreased H-H distance, elevating the energy of the H 1s SALC because of the local antibonding character. The resulting $\sigma_{C\text{-}H}$ bonding orbital therefore has greater nonbonding (pure C 2p) character as the angle decreases, made evident visually by the 30° angle case in Fig. 3C. Conversely, larger bond angles lead to a more stabilized SOMO with greater contribution from H orbitals. This picture is consistent with the observed increase in the 1s → SOMO x-ray probe excitation energy with decreasing bond angle shown in Fig. 3B. The x-ray oscillator strength also increased with a decrease in bond angle (supplementary materials). This behavior of the oscillator strength highlighted the increase in C 2p character of the SOMO because transitions from the C 1s level to other possible valence atomic orbitals that may contribute to the SOMO, such as C 2s or H 1s, have negligible oscillator strength. Therefore, the XTAS signal revealed the extent to which the SOMO lost C-H bonding character during the relaxation process.

It is thus apparent that the $T_d \rightarrow C_{2v}$ JT distortion activates scissoring motion about the smallest bond angle in the C_{2v} minimum, which was the most evident feature in the x-ray spectra. Furthermore, the frequencies indicated in Fig. 1C suggest that the asymmetric scissoring mode is activated to a greater extent than the symmetric scissoring mode. The greater activation of the asymmetric scissoring mode is further supported by the short time (<10 fs) evolution of the molecular bond angles (supplementary materials), which revealed that the smallest H-C-H bond angle decreases over time, whereas the largest H-C-H bond angle increases in value. For a perfectly harmonic PES, the excess energy accumulated in this asymmetric scissoring mode would remain undissipated therein, leading to undamped oscillation of the XTAS signal and geometric parameters about the minimum before radiative relaxation to the vibrational ground state. However, the PES of CH_4^+ is highly anharmonic (see discussion above), and the surplus energy spreads out to all other modes. This redistribution was observed through damping in the oscillations for both the experimental XTAS signal CM1 and the mean geometric parameters from the AIMD trajectories (Figs. 2 and 3). In addition, considerable broadening of the XTAS signal was observed after the initial 10 fs, which was mirrored by an increase in the width of the probability distributions for the geometric parameters. Figure 2D indicates that the experimental XTAS CM1 oscillations had a damping lifetime of 58 fs, and oscillations in parameters computed from AIMD trajectories were mostly damped out within 60 fs (supplementary materials). It therefore appears that a large proportion of energy was transferred out of the JT-activated asymmetric scissoring mode to other internal degrees of freedom within this timescale, constituting an ultrafast example of intramolecular vibrational energy redistribution. This process can also be described in terms of dephasing of the asymmetric scissoring mode (i.e., relaxation

toward thermal equilibrium), which was ultimately reflected in the decoherence of the XTAS signal.

Comparison between experiment and theory revealed that the XTAS signal was reporting the nuclear motion over the duration of the relaxation process. It is important to consider that SFI experiments could potentially exhibit electronic relaxation dynamics without considerable nuclear motion, involving highly excited Rydberg or cationic states (*38*, *39*). To prove that the observed XTAS signal dynamics solely arose from nuclear (rather than electronic) relaxation, we performed experiments and computations for the dynamics after SFI of CD_4. Figure 4A presents the time evolution of the resulting experimental XTAS signal, and Fig. 4B shows the computed XTAS spectrum from OO-DFT on 255 AIMD trajectories of CD_4^+. The good agreement between experiment and theory further validated the ability of the computed trajectories to successfully simulate the experimental molecular dynamics. The greater mass of the deuterium isotope should slow the scissoring motion, leading to slower time evolution of the signal for CD_4^+ relative to CH_4^+. Figure 4C confirms this to be the case by comparing the time evolution of the CM1 for both CH_4^+ and CD_4^+ from experiment and theory. The time taken by the CM1 to reach the 281.5-eV value associated with the C_{2v} cation geometry was longer for CD_4^+ than for CH_4^+, and the effect of deuteration could be gauged by the ratio (CD_4^+/CH_4^+) of these times. This ratio was measured to be 1.4 ± 0.3 from experiment and calculated to be 1.44 ± 0.06 from theory (supplementary materials). The value thus calculated was close to the ratio between the asymmetric scissoring frequencies for the smallest bond angle in CH_4^+ and CD_4^+ (computed to be 1.34). However, it is important to note that all the normal modes of C_{2v} CH_4^+ have similar frequency ratios upon isotopic substitution (supplementary materials). Nonetheless, the slower dynamics observed for CD_4^+ unambiguously reveal that the signal was reporting on nuclear dynamics. We also note that Fig. 4C shows that the relaxation dynamics after JT distortion for CD_4^+ continue to be slower up to 45 fs, from both experiment and theory. Longer time behavior for the computed CD_4^+ XTAS signal is compared with CH_4^+ in the supplementary materials (up to 85 fs), revealing slower coherent oscillations in the signal CM1 for CD_4^+. We also note that Baker *et al.* (*21*) have reported that dynamics within the first 1.6 fs of ionization were a factor of 2 to 3 slower for CD_4^+ versus CH_4^+. This behavior at very short times resulted from the decay of the autocorrelation of the nuclear wave function (*9*, *21*), which is distinct from the longer time dynamics reported here involving substantial atomic displacements, therefore representing almost nonoverlapping nuclear wave functions.

Conclusions

CH_4^+ was prepared from SFI of CH_4 and probed with XTAS near the carbon K-edge with few-femtosecond time resolution. Evolution of the excitation from the C 1s level to the valence hole revealed the dynamics of JT symmetry breaking away from the parent T_d geometry, as well as subsequent coherent motion and dissipation of released energy out of active modes. All three of these aspects of intramolecular relaxation have been successfully observed and analyzed. The combination of experiment and theory revealed that the molecule first reached the JT-distorted form within 10 ± 2 fs after ionization. This distortion involved reduction of a H-C-H bond angle from 109.5° toward 55°, which was directly reported by a blue shift in the x-ray absorption signal. The JT dynamics were found to be 1.4× slower in deuterated methane on account of the larger substituent mass, proving that the observed dynamics arose from nuclear motions. The energy released by the JT distortion drove a few coherent oscillations in the activated modes before being distributed over other molecular internal degrees of freedom, leading to damping of the oscillations within 60 fs of ionization. We note that the observed behavior for CH_4^+ is distinct from that observed in previous XTAS studies (*26*, *28*) on the dynamics of CF_4^+ and CCl_4^+ because those species are highly unstable against bond dissociation. CF_4^+ has not been experimentally detected to date (*26*); metastable CCl_4^+ has been previously observed (*28*), but signals from the intramolecular relaxation pathways were unable to be disentangled from bond breaking. The subsequent coherence and dissipation of energy from the JT activated asymmetric scissoring mode to other internal degrees of freedom was only observed in CH_4^+. This work thus opens the door to studies on how ultrafast vibrational coherence influences the redistribution of excess energy in more complex systems.

REFERENCES AND NOTES

1. H. A. Jahn, E. Teller, *Proc. R. Soc. Lond. A* **161**, 220–235 (1937).
2. I. B. Bersuker, *Chem. Rev.* **101**, 1067–1114 (2001).
3. H. C. Longuet-Higgins, in *Advances in Spectroscopy*, H. W. Thompson, Ed. (Interscience Publishers, 1961), pp. 429–472.
4. I. Persson, P. Persson, M. Sandström, A.-S. Ullström, *Dalton Trans.* **7**, 1256–1265 (2002).
5. H. Köppel, L. S. Cederbaum, W. Domcke, *J. Chem. Phys.* **89**, 2023–2040 (1988).
6. A. W. Potts, W. C. Price, *Proc. R. Soc. Lond. A* **326**, 165–179 (1972).
7. L. B. Knight Jr., J. Steadman, D. Feller, E. R. Davidson, *J. Am. Chem. Soc.* **106**, 3700–3701 (1984).
8. R. Signorell, M. Sommavilla, F. Merkt, *Chem. Phys. Lett.* **312**, 139–148 (1999).
9. C. E. M. Gonçalves, R. D. Levine, F. Remacle, *Phys. Chem. Chem. Phys.* **23**, 12051–12059 (2021).
10. E. Hirota, *J. Mol. Spectrosc.* **77**, 213–221 (1979).
11. R. Signorell, F. Merkt, *J. Chem. Phys.* **110**, 2309–2311 (1999).
12. R. Signorell, F. Merkt, *Faraday Discuss.* **115**, 205–228 (2000).
13. H. J. Wörner, R. van der Veen, F. Merkt, *Phys. Rev. Lett.* **97**, 173003 (2006).
14. H. J. Wörner, X. Qian, F. Merkt, *J. Chem. Phys.* **126**, 144305 (2007).
15. T. Mondal, A. J. C. Varandas, *J. Chem. Phys.* **135**, 174304 (2011).
16. T. Mondal, A. J. C. Varandas, *J. Chem. Phys.* **137**, 214320 (2012).
17. P. Krause, S. Matsika, *J. Chem. Phys.* **136**, 034110 (2012).
18. T. Mondal, A. J. C. Varandas, *J. Chem. Phys.* **143**, 014304 (2015).
19. J. Rabalais, T. Bergmark, L. Werme, L. Karlsson, K. Siegbahn, *Phys. Scr.* **3**, 13–18 (1971).
20. P. Baltzer *et al.*, *Chem. Phys.* **196**, 551–567 (1995).
21. S. Baker *et al.*, *Science* **312**, 424–427 (2006).
22. M. Li *et al.*, *Nat. Commun.* **12**, 4233 (2021).
23. L. Varvarezos *et al.*, *Chem. Phys. Lett.* **775**, 138687 (2021).
24. L. Barreau *et al.*, *Sci. Rep.* **10**, 5773 (2020).
25. R. Geneaux, H. J. B. Marroux, A. Guggenmos, D. M. Neumark, S. R. Leone, *Phil. Trans. R. Soc. A* **377**, 20170463 (2019).
26. Y. Pertot *et al.*, *Science* **355**, 264–267 (2017).
27. K. S. Zinchenko *et al.*, *Science* **371**, 489–494 (2021).
28. A. D. Ross *et al.*, *Chem. Sci.* **13**, 9310–9320 (2022).
29. O. Smirnova, M. Spanner, M. Ivanov, *J. Phys. B At. Mol. Opt. Phys.* **39**, S307 (2006).
30. J. Schirmer *et al.*, *Phys. Rev. A* **47**, 1136–1147 (1993).
31. J.-J. Pireaux *et al.*, *Phys. Rev. A Gen. Phys.* **14**, 2133–2145 (1976).
32. C. Wu *et al.*, *Phys. Rev. A* **75**, 043408 (2007).
33. A. Ferré *et al.*, *J. Phys. B At. Mol. Opt. Phys.* **47**, 124023 (2014).
34. K. F. Chang *et al.*, *J. Chem. Phys.* **156**, 114304 (2022).
35. D. Hait, M. Head-Gordon, *J. Phys. Chem. Lett.* **12**, 4517–4529 (2021).
36. M. Paranjothy, R. Sun, Y. Zhuang, W. L. Hase, *WIREs Comput. Mol. Sci.* **3**, 296–316 (2013).
37. M. N. Paddon-Row, D. J. Fox, J. A. Pople, K. N. Houk, D. W. Pratt, *J. Am. Chem. Soc.* **107**, 7696–7700 (1985).
38. W. G. Scherzer, H. L. Selzle, E. W. Schlag, R. D. Levine, *Phys. Rev. Lett.* **72**, 1435–1438 (1994).
39. Y. Kobayashi *et al.*, *Phys. Rev. A* **101**, 063414 (2020).
40. E. Ridente, Data for "Femtosecond Symmetry Breaking and Coherent Relaxation of Methane Cations via X-ray Spectroscopy," data set, Zenodo (2023); https://doi.org/10.5281/zenodo.7743367.

ACKNOWLEDGMENTS

Funding: This work is funded by the US Department of Energy (DOE) Office of Science, Basic Energy Sciences (BES) Program, Chemical Sciences, Geosciences, and Biosciences Division, under contract no. DE-AC02-05CH11231, through the Gas Phase Chemical Physics program (E.R., E.A.H., A.D.R., D.M.N., and S.R.L.) and the Atomic, Molecular, and Optical Sciences program (D.H. and M.H.-G.). The instrument was built with funds from the National Science Foundation through NSF MRI 1624322 and matching funds from the Lawrence Berkeley National Laboratory, the College of Chemistry, the Department of Physics, and the Vice Chancellor for Research at UC Berkeley. This research used resources of the National Energy Research Scientific Computing Center, a DOE Office of Science User Facility supported by the Office of Science of the US DOE under contract no. DE-AC02-05CH11231 using NERSC award BES-ERCAP0020263. A.D.R. was additionally funded by the US DOE, Office of Science, Office of Basic Energy Sciences, Materials Sciences and Engineering Division, under contract no. DE-AC02-05-CH11231, within the Physical Chemistry of Inorganic Nanostructures Program (KC3103); by the W. M. Keck Foundation, grant no. 042982; and by the US Army Research Office under grant no. W911NF-20-1-0127. **Author contributions:** Experimental investigation: E.R., E.A.H., and A.D.R. Theoretical investigation: D.H. Experiment supervision: S.R.L. and D.M.N. Theory supervision: M.H.-G. Writing – original draft: E.R., D.H., and E.A.H. Writing – review & editing: E.R., D.H., E.A.H., A.D.R., M.H.-G., D.M.N., and S.R.L. **Competing interests:** The electronic structure calculations were performed in Q-Chem, which is partially owned by M.H.-G. The other authors declare no competing interests. **Data and materials availability:** All data needed to evaluate the conclusions in the paper are present in the paper or the supplementary materials. The experimental and theoretical data can be accessed on Zenodo (*40*).

SUPPLEMENTARY MATERIALS

science.org/doi/10.1126/science.adg4421
Materials and Methods
Figs. S1 to S25
Tables S1 to S3
References (*41*–*64*)

Submitted 23 December 2022; accepted 19 April 2023
10.1126/science.adg4421

Femtosecond symmetry breaking and coherent relaxation of methane cations via x-ray spectroscopy

Enrico Ridente, Diptarka Hait, Eric A. Haugen, Andrew D. Ross, Daniel M. Neumark, Martin Head-Gordon, and Stephen R. Leone

Science, **380** (6646), .
DOI: 10.1126/science.adg4421

Editor's summary
The Jahn-Teller (JT) effect is a fundamental mechanism of geometric relaxation that leads to symmetry breaking in nonlinear molecular systems in degenerate electronic configurations. Despite being responsible for a variety of phenomena observed in many fields, direct imaging of this effect with high spectral resolution has remained a grand challenge. Using a combination of state-of-the-art experimental and theoretical time-resolved x-ray absorption techniques, Ridente *et al*. successfully reconstructed the ultrafast (few-femtosecond) molecular dynamics arising from the JT distortion in the prototypical example of the methane cation, as well as subsequent coherence and dissipation of energy to other internal degrees of freedom. In the future, the presented techniques could be used to study the JT distortion and other related dynamics in ultrashort time scales in more complex systems. —Yury Suleymanov